"PROCESS": a systems code for fusion power plants - Part 1: Physics

M. Kovari*, R. Kemp, H. Lux, P. Knight, J. Morris, D.J. Ward

CCFE, Culham Science Centre, Abingdon, Oxon, OX14 3DB, UK
*Corresponding author. Tel.: +44 (0)1235-46-6427. E-mail address: michael.kovari@ccfe.ac.uk

Abstract

PROCESS is a reactor systems code – it assesses the engineering and economic viability of a hypothetical fusion power station using simple models of all parts of a reactor system, from the basic plasma physics to the generation of electricity. It has has been used for many years, but details of its operation have not been previously published. This paper describes some of its capabilities. PROCESS is usually used in optimisation mode, in which it finds a set of parameters that maximise (or minimise) a Figure of Merit chosen by the user, while being consistent with the inputs and the specified constraints. Because the user can apply all the physically relevant constraints, while allowing a large number of parameters to vary, it is in principle only necessary to run the code once to produce a self-consistent, physically plausible reactor model. The scope of PROCESS is very wide and goes well beyond reactor physics, including conversion of heat to electricity, buildings, and costs, but this paper describes only the plasma physics and magnetic field calculations.

The capabilities of PROCESS in plasma physics are limited, as its main aim is to combine engineering, physics and economics. A model is described which shows the main plasma features of an inductive ITER scenario. Significant differences between the PROCESS results and the published scenario include the bootstrap current and loop voltage. The PROCESS models for these are being revised. Two new models for DEMO have been obtained. The first, DEMO A, is intended to be "conservative" in that it might be possible to build it using the technology of the near future. For example, since current drive technologies are not yet mature, only 12% of the current is assumed to be due to current drive. Consequently it is a pulsed machine, able to burn for only 1.65 hours at a time. Despite the comparatively large size (major radius is 9 m), the fusion power is only 1.95 GW. The assumed gross thermal efficiency is 33%, giving just 465 MW net electric power. The second, DEMO B, is intended to be "advanced" in that more optimistic assumptions are made. Comparison of DEMO A and B with a reference ITER scenario shows that current drive and bootstrap fraction need the most extrapolation from the perspective of plasma physics.

Keywords: fusion reactor, thermonuclear, deuterium, tritium, economics

Contents

1. Introduction

Assessing the engineering and economic viability of a hypothetical fusion power station can best be done using a computer program that includes simple models of all parts of a reactor system, from the basic plasma physics to the generation and transmission of electricity – in other words, a reactor systems code. These codes are well-suited to parametric studies and the identification of reactor operating regimes, which can then be more thoroughly investigated with more computationally intensive modelling methods. The PROCESS code has been used for many years, in particular for the Power Plant Conceptual Study (1), but the details of its operation have not been previously published. This paper describes some of its capabilities in as much detail as is allowed by the space available, and the focus has been kept on the modules used for recent DEMO studies. It is hoped that the high level of detail in this paper will make it possible for the algorithms in PROCESS to be evaluated and improved by collaboration with other institutions.

The code was based originally on TETRA (Tokamak Engineering Test Reactor Analysis) (2), which, together with much of the original version of PROCESS itself, was written at Oak Ridge National Laboratory, with contributions from other U.S. laboratories.

PROCESS has two modes of operation. In the *non-optimisation mode* the code finds a single set of parameters that are consistent with the inputs and the specified constraints. It does this by adjusting a set of variables known as iteration variables. This solution is unlikely to be unique. In *optimisation mode* PROCESS finds a set of parameters that maximise (or minimise) a Figure of Merit chosen by the user (Table 1), while being consistent with the inputs and the specified constraints. Given the large parameter space available, it is quite possible that the solution is a local rather than a global optimum, so it will depend on the starting values chosen.

It is useful to be able to scan through a range of values of a given parameter to see what effect this has on the machine as a whole. Scans are always carried out in optimisation mode. For the first run the iteration variables initially take the values specified in the input file, before being adjusted. In subsequent runs these variables are initialised to the values produced at the end of the previous run. The variable being scanned is incremented in each run. This method is intended to ensure that the machine parameters vary smoothly.

Because the user can apply all the physically relevant constraints, while allowing a large number of parameters to vary, it is in principle only necessary to run the code once to produce a self-consistent, physically plausible reactor model. The code does not need external routines or libraries. The user manual (3) explains not only how to use the code but how to add additional variables and equations, although it is intended to maintain a reference version of the code at CCFE. At present all users run a single version of the code on CCFE computers.

Many other systems codes have been developed – for example HELIOS (4), TREND (5) and SYCOMORE (6). The scope of PROCESS is very wide and goes well beyond reactor physics, including pumping, conversion of heat to electricity, buildings and costs. This paper describes only the plasma physics and magnetic field calculations, and does not discuss current limits for superconductors, stress limits for coil structures, etc. (Part 2, a paper on the engineering and economic modules, is in preparation.) We describe PROCESS version r326.

Table 1 Figures of Merit. The iteration variables can be adjusted to maximise (or minimise) one quantity chosen from this list.

capital cost (direct cost or constructed cost)
cost of electricity
divertor heat load
neutron wall load
plasma aspect ratio
plasma major radius
power injected by the heating and current drive systems
pulse length
ratio of fusion power to input power
ratio of fusion power to power injected by the heating and current drive systems
toroidal field on axis

2. Options, constraints and code design

PROCESS has modules for many different basic fusion variants, including stellarators, inertial confinement, D-^{3}He fusion and hydrogen production. As this paper is focussed on the routines used for DEMO studies, only the well-developed conventional aspect ratio DT tokamak modules are described in this paper.

There are two types of constraints in PROCESS: consistency equations and inequalities. In the non-optimisation mode only the consistency equations are enforced. In the more commonly used optimisation mode, both consistency equations and inequalities are enforced. In both cases, only those constraints specified by the user are implemented. There are several hundred input parameters, but one hundred of these are available as iteration variables. The number of iteration variables chosen must be greater than the number of constraints. The optimisation routine varies the chosen iteration variables between specified bounds to optimise the figure of merit within the constraints. Any of the inequalities listed can be redefined as an equality by the user. For pulsed reactors, all quantities are evaluated at the highest value they reach during the pulse, unless otherwise stated. Only single and double-null divertor configurations (with one and two divertors respectively) are included.

The order of calculations is not always intuitive. The parameters whose initial values need to be defined at the start of the run include:

- electron density
- toroidal field on axis
- plasma size and shape
- profile indexes
- total plasma β
- fuel composition and impurity fractions
- safety factor at 95% surface, q_{95}
- Central Solenoid (CS) overall current density at the end of the flat-top burn period (EOF)
- density of hot ions due to input of energy from neutral beams
- The density of thermal helium ions as a fraction of the electron density

These parameters are available to be chosen as iteration variables, except for the thermal helium density.

3. Glossary and Symbols

Table 2. Glossary of terms

BOF	Beginning of Flattop
BOP	Beginning of Pulse
CS	Central Solenoid (ohmic heating coil)
Current drive	Methods for generating plasma current other than induced voltage and bootstrap current
EOF	End of Flat-top
Flat-top	Time during which the plasma is in an approximately steady-state, the plateau.
Flux swing	The change in magnetic flux linked by the plasma, equal to the time integral of the loop voltage
PF coil	Poloidal field coil (not including the CS)
Separatrix	Last closed flux surface, last closed magnetic surface
Shield	Radiation shield outside the blanket
TFC	Toroidal field coil

Table 3. Symbols used. Other symbols are defined where they are used.

a	minor radius of plasma
A	aspect ratio
B_t	toroidal magnetic field on the geometric axis
B_p	poloidal magnetic field averaged over the plasma perimeter
I_p	toroidal plasma current
l_i	normalised internal inductance of the plasma (see 9.1)
$<n_e>$	volume averaged electron density
$<n_e>_{la}$	line-averaged electron density
$<n_f>$	fuel ion density (D + T)
$<n_{it}>$	total thermal ion density
$<n_\alpha>$	thermal alpha (^{4}He) density
N_{TF}	number of TF coils
P_α	mean alpha power created per unit volume by fusion
P_{inje}	auxiliary power deposited in the electrons (see 12)
P_{inji}	auxiliary power deposited in the ions (see 12)
q_{95}	plasma safety factor at the 95% flux surface
$<T_e>$	volume averaged electron temperature
$<T_e>_n$	density-weighted average electron temp
$<T_i>$	volume averaged ion temperature
$<T_i>_n$	density-weighted average ion temperature
R	major radius
V	plasma volume
β	Total plasma beta
β_p	Poloidal plasma beta (see 15)
δ	plasma separatrix triangularity
ε	Inverse plasma separatrix aspect ratio
κ	plasma separatrix elongation

4. Plasma profiles

Two plasma profile options are available: without pedestal (the default), and a new model with a pedestal, which may be appropriate for an H-mode plasma. Not all the physics routines take account of the profile, however. The only models that use pedestal profiles in a fully self-consistent way are fusion power, lower hybrid current drive, and electron cyclotron current drive. The following models are based on specific profiles with no variable parameters: loop resistance, neutral beam shine-through and neutral beam current drive. The models for radiation (see section 10), "equilibration power" (4.1), and thermal β (15) use the no-pedestal profile.

For calculating integrated and peak values the plasma cross-section is taken to be elliptical, where ρ is the normalised minor radial co-ordinate, which can be expressed in xy coordinates whose origin is on the plasma centre:

$$\rho = \frac{1}{a}\sqrt{x^2 + \left(\frac{y}{\kappa}\right)^2}.$$

Except for the area close to the X-point, ρ^2 is an approximation to the conventional poloidal flux coordinate, normalised to unity at the separatrix.

4.1. Without pedestal

The profiles are of the following form:

Density	$n(\rho) = n_0(1-\rho^2)^{\alpha_n}$
Temperature	$T(\rho) = T_0(1-\rho^2)^{\alpha_T}$
Current density	$\mathrm{J}(\rho) = J_0(1-\rho^2)^{\alpha_J}$

The density and temperature profile exponents are specified by the user, and n_0, T_o, and J_0 are the density, temperature and current density at the magnetic axis. The current density exponent can be set by the user, or given (7 p. 110) by

$$\alpha_J = \frac{q_{cyl}}{q_0} - 1\,,$$

where q_0 is the central safety factor, and q_{cyl} is the cylindrical equivalent safety factor, given (8) by

$$q_{cyl} = 5\frac{B_t a^2}{RI_p}\frac{\left(1+\kappa_{95}^2\left(1+2\delta_{95}^2-1.2\delta_{95}^3\right)\right)}{2}$$

(units T, MA, m), where κ_{95} and δ_{95} are given in section 7.
It can be shown that the electron and ion temperatures and the electron density at the magnetic axis are:

$$T_{0e} = \langle T_e\rangle(1+\alpha_T)$$
$$T_{0i} = \langle T_i\rangle(1+\alpha_T)$$
$$n_{0e} = \langle n_e\rangle(1+\alpha_n).$$

The pressure profile coefficient is

$$\alpha_p = \alpha_n + \alpha_T.$$

Note these profiles are not used for evaluating plasma volume or area; the Shafranov shift (the offset between the geometrical centre and the magnetic centre) is not included; and there is no pedestal (edge transport barrier) in this version of the code. The profile factor, which relates volume-averaged with density-weighted quantities, is:

$$P_{coef} = \frac{\langle T_e\rangle_n}{\langle T_e\rangle} = \frac{\langle T_i\rangle_n}{\langle T_i\rangle} = \frac{(1+\alpha_n)(1+\alpha_T)}{1+\alpha_n+\alpha_T}$$

The line-averaged electron density (averaged along a major radius from the edge to the centre of the plasma) is:

$$\langle n_e\rangle_{la} = \frac{n_{0e}}{2}\frac{\Gamma\left(\frac{1}{2}\right)\Gamma(\alpha_n+1)}{\Gamma\left(\alpha_n+\frac{3}{2}\right)} = 0.886227\langle n_e\rangle(1+\alpha_n)\frac{\Gamma(\alpha_n+1)}{\Gamma\left(\alpha_n+\frac{3}{2}\right)}\,,$$

where Γ is the gamma function.

The volume-averaged electron and ion temperatures are equal by default, but a ratio other than one can be input. If they are different, the power per unit volume transferred between ions and electrons (the "equilibration power") is calculated:

$$P_{ie} = 2.42165\ 10^{-41}\Lambda_{\mathrm{ie}}\langle n_e\rangle^2\langle Z_{eff}\rangle_n\frac{\langle T_i\rangle - \langle T_e\rangle}{\langle T_e\rangle^{3/2}}\frac{(1+\alpha_n)^2}{\left(2\alpha_n-\frac{1}{2}\alpha_T+1\right)\sqrt{1+\alpha_T}}$$

where $\langle Z_{eff}\rangle_n$ = density weighted plasma effective charge, and the ion-electron Coulomb logarithm is calculated here as

$$\Lambda_{\mathrm{ie}} = 31 - \frac{\ln\langle n_e\rangle}{2} + \ln\langle \mathrm{T_e}\rangle$$

(units m^{-3}, eV).

4.2. With pedestal

The density profile is

$$n(\rho) = \begin{cases} n_{ped} + (n_0 - n_{ped}) \left(1 - \dfrac{\rho^2}{\rho_{ped,n}^2}\right)^{\alpha_n} & 0 \le \rho \le \rho_{ped,n}, \\ n_{sep} + (n_{ped} - n_{sep}) \left(\dfrac{1-\rho}{1-\rho_{ped,n}}\right) & \rho_{ped,n} < \rho \le 1, \end{cases}$$

and the temperature profile is

$$T(\rho) = \begin{cases} T_{ped} + (T_0 - T_{ped}) \left(1 - \dfrac{\rho^{\beta_T}}{\rho_{ped,T}^{\beta_T}}\right)^{\alpha_T} & 0 \le \rho \le \rho_{ped,T}, \\ T_{sep} + (T_{ped} - T_{sep}) \left(\dfrac{1-\rho}{1-\rho_{ped,T}}\right) & \rho_{ped,T} < \rho \le 1, \end{cases}$$

where subscripts 0, *ped* and *sep*, denote values at the centre ($\rho = 0$), the pedestal ($\rho = \rho_{ped}$) and the separatrix ($\rho = 1$), respectively. The density and temperature peaking parameters α_n and α_T and the second exponent β_T in the temperature profile can be chosen by the user. Note that density and temperature can have different pedestal positions $\rho_{ped,n}$ and $\rho_{ped,T}$. The volume-averaged density $\langle n_e \rangle$ and temperature $\langle T_e \rangle$ are inputs (or iteration variables), and the density n_0 and temperature T_0 at the centre are given by

$$\begin{aligned} n_0 \;=\; & \frac{1}{3\rho_{ped,n}^2} \left[3\langle n_e \rangle (1+\alpha_n) + n_{sep}(1+\alpha_n)(-2+\rho_{ped,n}+\rho_{ped,n}^2)\right. \\ & \left. -n_{ped}((1+\alpha_n)(1+\rho_{ped,n}) + (\alpha_n - 2)\rho_{ped,n}^2)\right] \end{aligned}$$

$$T_0 = T_{ped} + \left[T_{ped}\rho_{ped,T}^2 - \langle T_e \rangle + \frac{1}{3}(1-\rho_{ped,T})\left[(1+2\rho_{ped,T})T_{ped} + (2+\rho_{ped,T})T_{sep}\right]\right]\gamma$$

where

$$\gamma = \begin{cases} \dfrac{-\Gamma(1+\alpha_T+2/\beta_T)}{\rho_{ped,T}^2 \Gamma(1+\alpha_T)\Gamma((2+\beta_T)/\beta_T)} & \text{if } \alpha_T \text{ is integer} \\ \dfrac{\Gamma(-\alpha_T)\sin(\pi\alpha)\Gamma(1+\alpha_T+2/\beta_T)}{\pi\rho_{ped,T}^2 \Gamma((2+\beta_T)/\beta_T)} & \text{if } \alpha_T \text{ is not integer} \end{cases}$$

and Γ is the gamma function. The pedestal model is used with equal electron and ion temperatures.

5. Poloidal field and poloidal field coils

A tokamak requires a set of poloidal field (PF) coils and usually a central solenoid (CS). A pair of coils directly above and below the plasma "pulls" on the plasma in order to elongate it. One or more pairs of coils with larger major radius provide an approximately vertical field to overcome the bursting force due to the plasma current. The layout allowed by PROCESS is shown in Figure 1. The PF coils are numbered 1 to 3, but several coils of type 3 are permitted. Each pair of coils is symmetric about the midplane except coil 2 in the case of a single-null plasma.

5.1. Vertical Field

The vertical vacuum field required at the major radius to maintain the plasma in equilibrium is

$$B_z = -\frac{\mu_0 I_p}{4\pi R}\left(\ln\left(\frac{8R}{a}\right) + \beta_p + \frac{l_i}{2} - \frac{3}{2}\right).$$

This is consistent with ref (7). This equilibrium field is assumed to be generated by a set of vertical field coils (shown as number 3 in Figure 1), together with the CS. Coil 1 is assigned a nominal equilibrium current of zero. Coil 2 creates the elongated shape of the plasma, using a current given by

$$I_{cls2} = 2I_p\left(1 - \frac{\kappa a}{Z_2}\right),$$

where Z_2 is the half-height of the coil. For plasma initiation the code calculates the currents in <u>all</u> the PF coils required to achieve as near as possible zero magnetic field in the poloidal plane, in the presence of the field from the CS, at 32 points equally spaced across the plasma midplane. To do this the code finds a least squares best fit solution to an over-determined set of linear algebraic equations, using singular value decomposition. The magnetic

field at any point due to a number of co-axial circular current filaments is calculated using standard formulae involving elliptic integrals (9).

5.2. PF coils and CS: size and location.

The half-height of the CS is given by

$$h_{CS} = h_{max} O_{hhghf}$$

where h_{max} = inside height of TFC, and O_{hhghf} is defined by the user in the range (default value 0.71). Increasing the height of the CS increases the flux swing available. The vertical position of each of the number 3 coils is calculated relative to the minor radius, using a user-specified array Z_{ref}:

$$Z_3(i) = aZ_{ref}(i)$$

The number 3 coils are placed on a sphere whose radius is

$$R_{clsnorm} = R_{tot} + \frac{tfthko}{2} + R_{outr}$$

The radius of each coil in this family is then

$$R_3 = \sqrt{R_{clsnorm}^2 - Z_3^2}$$

Coils 2 and 3 have square cross-sections.

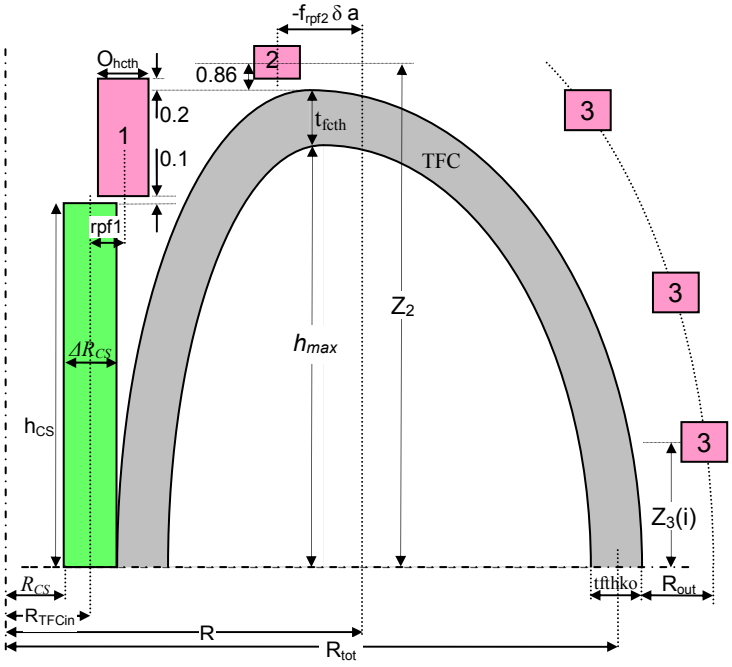

Figure 1. Geometry of CS and PF coils. The TF coil is also shown. Dimensions m.

The peak field at the CS, which plays a major part in determining the pulse length available in a pulsed reactor, is calculated using data from (10). First, the field in the centre of the CS is given by

$$B_0 = \mu_0 a J \beta \ ln\left(\frac{\alpha + \sqrt{\alpha^2 + \beta^2}}{1 + \sqrt{1 + \beta^2}}\right)$$

where

$$\alpha = \frac{R_{CS} + \Delta R_{CS}}{R_{CS}}$$

$$\beta = \frac{h}{R_{CS}}$$

and J = current density, R_{CS} = solenoid inner radius, $R_{CS}+\Delta R_{CS}$ = solenoid outer radius, and h = solenoid half height.

Then the maximum field, which occurs on the inside edge of the coil, is derived using fits given in (10). The fits are intended to be valid provided

$$\frac{\text{outer radius}}{\text{inner radius}} < 2 \;\; and \;\; \frac{\text{half-height}}{\text{inner radius}} > 0.5$$

Using a more general but less accurate method the code calculates the total field due to all the PF coils, CS and plasma, at the inside and outside faces of any specified PF coil, or the plasma. The field due to the CS at the other coils is calculated by modelling the CS as a number of equally spaced infinitely thin current loops ("filaments"), whose radius is the mean of the inner and outer radii of the CS. The current density in the CS is an input (and is available as an iteration variable).

Each PF coil is treated as a single thin filament, except for the coil at which the field is being calculated. This coil is divided into 4 equal pieces, each of which is treated as a filament. The plasma is treated as a thin filament at the major radius. Figure 2 shows the simplifications used. The B field components at the inner and outer field points for each coil in the the group (ie the upper and lower coils of a PF pair) are calculated.

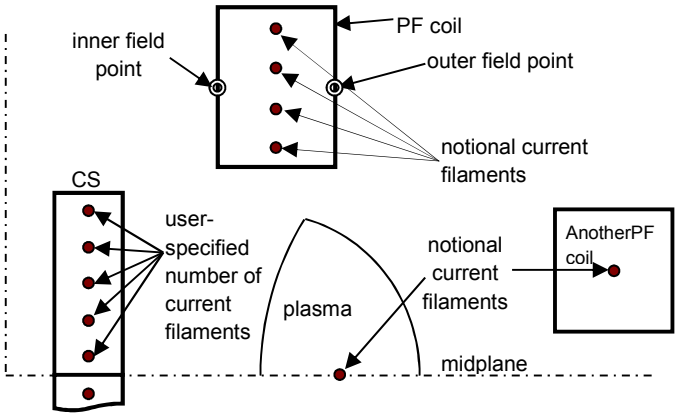

Figure 2. Model of currents used to calculate field at inner and outer radii of a PF coil

6. Toroidal Field Coil

When neutral beams are used, the beams must pass at an angle between the TF coils. This imposes a limit to the maximum tangency radius, which can be imposed as a constraint. Increasing the number of coils (N_{TF}) will reduce the field ripple but may also reduce the achievable tangency radius. Limitations on the number of coils due to the need to remove the blanket modules through ports between the coils are not taken into account at present.

6.1. TF coil ripple

Since discrete TF coils are used, the magnetic field will have a toroidal variation, known as ripple, which can cause losses of fast alphas, neutral beam particles, and even affect the confinement of thermal plasma. These losses will not only affect the power balance, but may create unacceptable localised heat loads. At present these effects are not modelled in the code, but the user can specify the maximum permissible ripple at the outer edge of the plasma, δ_{max}, where ripple δ is defined as

$$\delta = \frac{B_{max} - B_{min}}{B_{max} + B_{min}},$$

and B_{max} and B_{min} are the maximum and minimum values of the toroidal component of the field at the outer edge of the plasma in the midplane. PROCESS checks whether the calculated ripple is acceptable. The calculated value of ripple amplitude at the plasma edge in the midplane is estimated using a fitting function derived from calculations by the authors for coils of different shapes. The calculations used the Biot-Savart law, modelling each TF coil as a set of filaments. The curved section of each filament was divided into short sections, which were modelled as infinitesimal straight wires. The vertical part of each filament was modelled as a single straight wire of finite length (10 pp. 38-39). The following fit was derived:

$$\delta = (0.875 - 0.0557x)\left(\frac{R+a}{R_{tot}}\right)^{N_{TF}-(1.617+0.0832x)}$$

where x, the dimensionless coil width is

$$x = \frac{w_{wp}}{R} N_{TF},$$

R_{tot} = radius to the centre of the outer TF coil leg (Figure 1) (m),
w_{wp} = the toroidal width of the winding pack of the TF coil (the conducting portion of the coil),
and the range of applicability of the fit is

$$0.737 < x < 2.95$$

$$16 < N_{TF} < 20$$

$$0.7 < (R + a)/R_{tot} < 0.8$$

If the ripple is excessive the radius of the outer leg of the TFC is increased appropriately. We can compare this fit with a simpler formula from (7), shown in Figure 3.

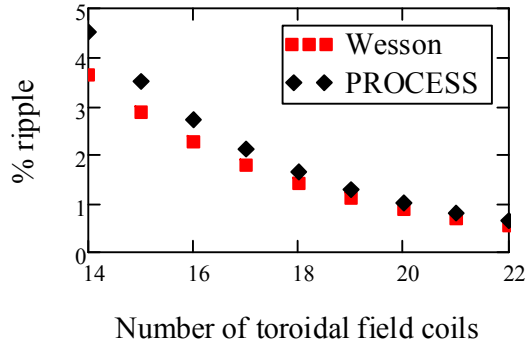

Figure 3. Ripple at the outer edge of the plasma calculated using PROCESS formula, compared to formula from **(7)**. R=9 m, a=2.381 m, outer leg radius R_{tot} = 14.42 m

6.2. TF coil fields

The peak field at the superconductor determines the maximum current density, which in turn determines the space available for the steel case, and so on. The TF coil is assumed to consist of a winding pack, which contains the conductor, surrounded on all sides by a case. The peak field due to the TF coils will be at the plasma-facing side of the winding pack in the inboard leg. If the field was toroidally symmetric it would be given by Ampère's law:

$$B_{nom} = \frac{\mu_0}{2\pi}\frac{I_{TFC}}{R_{Bmax}}$$

where I_{TFC} = total current in the TF coils, and R_{Bmax} = the radius of the peak field. The peak field at the conductor is estimated using a fitting function derived using the Biot-Savart law as described in 6.1. Two dimensionless input parameters were used:

dimensionless coil width: $t = w/w_{max}$

Dimensionless coil thickness: $z = \Delta r/w_{max}$

where

w is the toroidal width of the plasma-facing face of the inboard leg,

w_{max} is the maximum coil width before coils touch:

$$w_{max} = 2(r_{in} - 0.5\Delta r)\tan\left(\frac{\pi}{N_{TF}}\right)$$

r_{in} = major radius of the centre of winding pack of the inboard leg,

Δr = radial thickness of winding pack,

The fit is

$$B_{maxTFrp} = B_{nom}(a_1 + a_2 e^{-t} + a_3 z + a_4 z t)$$

The coefficients a_1 to a_4 are:

16 coils: 0.3272, 1.972, -1.233, 1.142

18 coils: 0.371, 1.952, -1.414, 1.066

20 coils: 0.303, 2.027, -1.135, 1.091

The limits of applicability are $0.3 < t < 1$, and $0.26 < z < 0.7$. In practice optimisation will usually make the winding pack fill the toroidal width available in the inboard leg, in which case the correction to the toroidally symmetric field is negligible.

The field on the plasma axis, B_t, is available as an iteration variable, and the correct current is guaranteed provided the following constraint equation is applied:

$$B_t = B_{nom} \frac{R_{Bmax}}{R}.$$

Stored energy per coil:

$$E_{stoTF} = \frac{1}{2} \frac{L_{TF}}{N_{TF}} I_{TF}^2,$$

where L_{TF} is the self-inductance of the entire set of TF coils (considered as a single axisymmetric turn). It is calculated by numerical integration over the cross-sectional area:

$$L_{TF} = \int B(r) 2h dr,$$

where the vacuum field inside the coil for unit current is given by

$$B(r) = \frac{\mu_0}{2\pi r},$$

h is the height from the midplane to the inside of the TF coil, and r is the major radius coordinate. The additional contribution from the cross-sectional area of the coil itself is calculated by taking the field within the coil thickness as *B(r)/2*.

7. Plasma geometry

A vertically elongated plasma has a larger poloidal circumference for given major radius, giving a bigger safety factor, and makes it easier to create an X-point for divertor operation. Unfortunately, this makes the plasma vertically unstable, requiring both passive and active control. PROCESS provides an estimate for the maximum elongation that can be controlled in a stable manner (5):

$$\kappa = 1.5 + \frac{0.5}{A - 1} \quad (A \geq 2).$$

The triangularity and elongation of the 95% flux surface are smaller than those of the separatrix, and are given (11) by

$$\kappa_{95} = \frac{\kappa}{1.12} \quad and \quad \delta_{95} = \frac{\delta}{1.5}.$$

The plasma volume is found by integrating between two circular arcs. The centres (C_1, C_2), radii (R_{c1}, R_{c2}) and integrated volumes (V_{out}, V_{in}) of the arcs are given by

$$Z_n = \kappa a$$

$$R_{c1} = \frac{(R + a)^2 - (R - \delta a)^2 - Z_n^2}{2(1 + \delta)a}$$

$$R_{c2} = \frac{-(R - a)^2 + (R - \delta a)^2 + Z_n^2}{2(1 - \delta)a}$$

$$C_1 = R + a - R_{c1}$$

$$C_2 = -R + a + R_{c2}$$

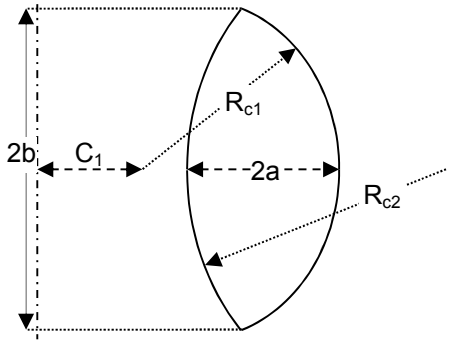

Figure 4. Calculation of plasma volume and surface area.

The plasma volume, surface area, cross-sectional area and poloidal perimeter (used only for calculating the mean poloidal field along the perimeter in section 15), are calculated using this geometry. The volume is multiped by a user-specified correction factor (usually 1).

By default the first wall area is calculated as the sum of two half toroids, whose major radius is in both cases given by that of the top of the plasma:

$$R_1 = R - a\delta \ .$$

The minor radius of the inboard toroid segment is

$$R_1 - (R - a - \Delta_{SOLinboard}),$$

where $\Delta_{SOLinboard}$ is the clearance between the separatrix and the first wall on the inboard side.
The minor radius of the outboard toroid segment is

$$R + a + \Delta_{SOLoutboard} - R_1,$$

where $\Delta_{SOLoutboard}$ is the clearance between the separatrix and the first wall on the inboard side. The first wall area is the sum of the areas of the two half toroids, multiplied by a user-specified coverage factor which can be used to take account of the area occupied by the divertor, heating ports and so on:

$$(1 - f_{hole}).$$

8. Heating and current drive

In a steady-state reactor all the current must derive from a combination of bootstrap current and current drive, and even an inductively driven reactor may benefit from additional current drive. This section gives the algorithms used for neutral beam and electron cyclotron current drive techniques. There are lower hybrid models in PROCESS, but they are not often used.

For bootstrap current, the formulae by Sauter *et al* (12) are being incorporated as the default model, but several other scalings are available. Whichever option is chosen, the bootstrap current fraction is constrained to be less than or equal to the total fraction of the plasma current produced by non-inductive means, as specified by the user.

8.1. Neutral beams

Several models for neutral beam current drive are available, but only the default formulation is given here. Ref (13) compares a range of codes, using ITER values. These results are given in Table 4, together with PROCESS values for an approximately similar scenario. Plasma rotation is not taken into account. The PROCESS result lies near the average of the results listed.

Table 4
Neutral beam current drive comparison (13), based on the ITER steady-state scenario 1, from (14).

Code	Neutral beam current drive, MA
PROCESS (default NBI model)	2.43
OFMC	2.83
ACCOME	2.31
ONETWO/NUBEAM	2.13
ASTRA	2.83
NEMO/SPOT	1.73

The path length d_{path} travelled by the beam between entering the plasma and the point at which it is tangent to the major radius is calculated as follows (see Figure 5). The beam is in the midplane (so-called "on-axis injection").

$$d_{path} = \sqrt{(R + \varepsilon R)^2 - (R\, f_{rbeam})^2}$$

where f_{rbeam} = tangency radius / plasma major radius.

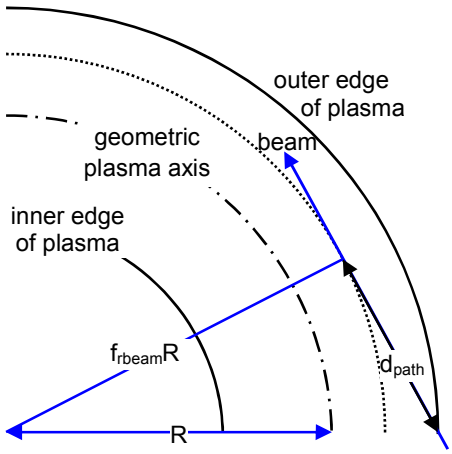

Figure 5. Geometry for calculating the distance travelled by the neutral beam

The number of exponential decay lengths traversed by the beam to its tangency point is:

$$\tau_{beam} = d_{path}\langle n_e \rangle \sigma_{stop}$$

where σ_{stop} is the the beam stopping cross-section. Mikkelsen and Singer (15) found that the current driven by a deuterium beam is greatest when $2 \leq \tau_{beam} \leq 4$. At higher values of τ the beam deposition in the plasma core falls due to poor penetration, and for lower values the shinethrough loss becomes significant. The shine-through fraction is:

$$f_{shine} = e^{-2 d_{path}\langle n_e \rangle \sigma_{stop}}.$$

PROCESS does not yet have an explicit constraint on shine-through, but the user can specify the attenuation factor from the entry point to the tangency point. The beam stopping cross-section is estimated using an analytic fit from (16), suitable for for multiple impurities. PROCESS uses volume-averaged quantities. The dependences of the cross-section on n_e and T_e are relatively weak, so it is reasonable to use volume averaged values of n_e and T_e. The dependence on the beam energy, however, is strong, so the use of the initial beam energy will cause the calculated cross-section to be too small.

The beam current drive follows the 1990 ITER formulation (17), based on (15). The shine-through fraction is neglected. The current drive in this formulation is proportional to the ratio of tangency radius to major radius, even if this is greater than 1. The current drive efficiency is:

$$\eta_{nbss} = \frac{R_{tang}}{R} f_{effCD} \eta_{nb} \qquad \text{(equation 1)}$$

where
R_{tang} = beam tangency radius,

f_{effCD} = a user-specified adjustment factor for current drive efficiency, and

$$\eta_{nb} = A_{bd}\frac{5}{R}\frac{\langle T_e\rangle_n}{\langle n_e\rangle}\frac{J}{0.2}F,$$

(units m, keV, 10^{19}m^{-3}) where A_{bd} is a calibration factor based on more detailed models (18), given by

$$A_{bd} = 0.107(1 - 0.35\alpha_n + 0.14\alpha_n^2)(1 - 0.21\alpha_T)\left(1 - 0.2E_{nbeam} + 0.09{E_{nbeam}}^2\right),$$

where E_{nbeam} = initial neutral beam energy (keV), and the scaling factors J and F are given by

$$J = \frac{x^2}{4 + 3y + x^2(x + 1.39 + 0.61y^{0.7})}$$

$$F = 1 - \frac{1 - G}{Z_{eff}},$$

where

$$x = \sqrt{\frac{E_{nbeam}}{E_{crit}}}$$

$$y = 0.8\,Z_{eff}/A_{beam}$$

$$G = \left(1.55 + \frac{0.85}{Z_{eff}}\right)\sqrt{\varepsilon} - \left(0.2 + \frac{1.55}{Z_{eff}}\right)\bar{\varepsilon}$$

$$\bar{\varepsilon} = \frac{\varepsilon}{2}.$$

E_{crit} is the critical energy at which the ions and the electrons are heated equally by the beam ion, given here by the approximation (19):

$$E_{crit}(keV) = 10A_{beam}\langle T_e\rangle_n$$

where A_{beam} = atomic mass of the beam (amu). This current drive model is stated to apply when $n_{DT}/n_e \geq 0.9$, but this will not apply in a power plant, where the presence of helium ash and high Z impurities will make this ratio of the order of 0.7.

The atomic number of the beam is assumed to be 1. The factor $(1 - f_{shine})$ used by (15) and (11) has been omitted. The factor R_{tang}/R in equation 1was introduced by (15) as an approximation to the value of $v_\parallel/v$ at the point where the beam atoms enter the plasma, where $v_\parallel$ and v are the components of the beam atom velocity parallel and perpendicular to the local magnetic field, but this is only acceptable even as a rough approximation provided the factor is less than one. Other models have found that optimum current drive efficiency can sometimes be obtained when the beam tangency point is outside the plasma axis.

The total fraction of the plasma current produced by non-inductive means, $f_{vsbrnni}$, is an input, and is available as an iteration variable. The fraction of plasma current produced by auxiliary current drive is then just the remainder after the bootstrap current fraction f_{BS} is subtracted:

$$f_{accd} = f_{vsbrnni} - f_{BS}$$

The injection power required to drive the specified current is:

$$P_{NBeam} = \frac{f_{accd}I_p}{\eta_{nbss}}$$

The user can specify additional heating power not used for current drive.
The normalised current drive efficiency parameter is defined as

$$\gamma = \eta_{nbss}\,R\,\langle n_e\rangle$$

(units m, AW^{-1}, 10^{20}m^{-3})
The total injected power is broken down into power delivered to the ions and electrons, based on an extension of the approach in (7).

8.2. Electron Cyclotron heating and current drive

The electron cyclotron current drive option is not state-of-the-art and is not commonly used, but two models are available: the Culham model (20), and the original simple TETRA model. The latter (2) is a special case of the result by Karney and Fisch (21). The current drive efficiency parameter is:

$$\eta_{EC} = 0.21 \frac{\langle T_e \rangle_n}{R\langle n_e \rangle \lambda_{ee}} f_{effcd},$$

where f_{effCD} = a user-specified adjustment factor for current drive efficiency, and
λ_{ee} is the electron-electron Coulomb logarithm and is given by

$$\lambda_{ee} = 31 - \frac{ln\langle n_e \rangle}{2} + \ln\langle T_e \rangle$$

(units A/W, keV, 10^{20} m^{-3}). All the electron cyclotron power is deposited in the electrons, and is given by

$$P_{eccd} = P_{inje} = f_{accd} \frac{I_p}{\eta_{EC}} + P_{heat},$$

f_{accd} = fraction of plasma current produced by auxiliary current drive, and
P_{heat} is optional additional heating power not used for current drive.

9. Pulsed reactors and reactor start-up

PROCESS can model a steady-state reactor or a pulsed reactor. The cycle of a pulsed reactor is illustrated in Figure 6.

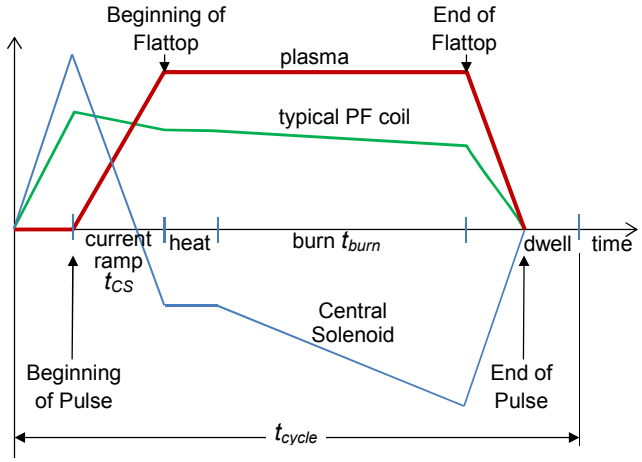

Figure 6. IIllustration of the current waveforms and the reactor cycle.

When the plasma current is ramped up too quickly, kink and tearing instabilities can occur, so in (22) a constraint on the rate of change of plasma current is proposed. If we assume that this maximum rate will be proportional to the final plasma current, we obtain

$$\frac{dI_p(t)}{dt} < 0.0455\ second^{-1} I_p(Flattop),$$

In the default case, the ramp-up time is simply given by setting the rate of change equal to this maximum, or it can be set by the user. The minimum inductive current ramp-up time depends on the voltage available from the CS power supply and the inductive coupling between the CS and the plasma:

$$t_{CSmin} = \frac{L_{CS}(I_{CS}(BOP) - I_{CS}(BOF))}{I_{CS}(BOP)R_{CS} - V_{PF} + L_{plasma,CS}\dot{I}_p}$$

where L_{CS} is the self-inductance of the CS,
$I_{CS}(t)$ is the CS current at time t, BOP is beginning of pulse, BOF is beginning of flattop,
R_{CS} is the resistance of the CS bus bars (assumed to include power supply),
V_{PF} = voltage of power supplies for CS and PF coils, taken to be the same for all coils
$L_{plasma,CS}$ = mutual inductance between CS and plasma, and

$\dot{I}_p$= maximum rate of change of plasma current shown above.
Optionally this constraint can be applied to the actual value of the ramp-up time: $t_{CS} > t_{CSmin}$.

9.1. Inductances

In a pulsed reactor the current in the CS and the PF coils is changed continuously to create a loop voltage, requiring knowledge of the self and mutual inductances of the coils and the plasma. The self-inductance of the CS is calculated from a formula for the inductance of a coil of any length and any rectangular cross-section (23):

$$L_{CS} = \mu_0 a n^2 \left\{ ln\left(\frac{8a}{R}\right)\left(1 + \frac{3R^2}{16a^2}\right) - \left(2 + \frac{R^2}{16a^2}\right)\right\}$$

where a = mean radius of winding, b = length, c = radial thickness, and R is approximated by

$$R = 0.2235(b + c).$$

The self-inductance of the plasma is the sum of so-called external and internal inductances,

$$L_p = L_{pext} + L_{pint}$$

where the external inductance L_{pext} is given in terms of the aspect ratio and elongation by a numerical fit from (24), and the internal inductance is expressed in terms of the normalised internal inductance l_i:

$$L_{pint} = \frac{\mu_0 R l_i}{2}.$$

The normalised internal inductance can be input, or given (7 p. 116) by

$$l_i = \ln\left(1.65 + 0.89\alpha_J\right).$$

9.2. Transformer flux swing

It is assumed that the plasma current is initially started by a loop voltage caused by electromagnetic induction, with no contribution from current drive. The consumption of flux during start-up and current ramp is given by sum of the resistive flux consumption during start-up and current ramp (Φ_{res}) and the flux consumption due to the self-inductance of the plasma during current ramp-up (Φ_{ind}). The calculation of Φ_{res} is based on the fact that the ramp-up takes of the order of the resistive current penetration time $\mu_0 a^2/\eta$, where η is the resistivity of the plasma. The flux consumption is therefore independent of the resistivity and the minor radius and is:

$$\Phi_{res} = C_E \mu_0 I_p R$$

where C_E is the empirical Ejima constant, defined by the user (default value 0.4). Flux consumption due to the self-inductance of the plasma (L_p, see 9.1) during current ramp-up is:

$$\Phi_{ind} = L_p I_p.$$

The PF coils are assumed to have zero current at time zero. The total change in flux caused by switching on the PF coils to their currents in the equilibrium (flat-top) phase is calculated using the mutual inductances, as

$$\Delta\Phi_{\mathrm{PF}} = \sum_{i=\ PF\ coils} L_{plasma,i} \frac{I_{eq,i}}{turns_i}$$

Where $L_{plasma,i}$ = mutual inductance between coil i and the plasma,
$I_{eq,i}$ = total current in PF coil i required to create the equilibrium vertical field in the absence of the CS, and
$turns_i$ = number of turns in PF coil i.
The flux swing required from the CS to ramp up the plasma current is then

$$\Delta\Phi_{\mathrm{CS}} = -(\Delta\Phi_{\mathrm{res}} + \Delta\Phi_{\mathrm{ind}}) - \Delta\Phi_{\mathrm{PF}}.$$

The change in the CS current will affect the vertical field, and currents in the PF coils need to be adjusted for this, causing an additional change in flux. To avoid carrying out a full solution to this problem, the CS is temporarily treated as infinitely long, and therefore has no external field. The current swing required in the CS can then be calculated:

$$\Delta I_{CS} = \frac{\Delta\Phi_{\mathrm{CS}}}{\Delta}$$

$$\Delta = \mu_0 \pi \left(\frac{R_{CS}^2 + \frac{1}{6}\Delta R_{CS}^2 + \frac{1}{2}\,\Delta R_{CS} R_{CS}}{2h_{CS}} \right)$$

where
h_{CS} = half-height of the CS
R_{CS} is the CS bore, and the additional terms in Δ correct for the finite thickness ΔR_{CS} of the CS coil.

The total CS current at end of flat-top is calculated from its cross-sectional area and the current density which is available as an iteration variable. The total flux swing needed for the entire pulse is:

$$\Phi_{tot} = \Phi_{res} + \Phi_{ind} + \Phi_{burn}$$

$$\Phi_{burn} = C_{sawth} V_{burn} t_{burn}$$

where V_{burn} = loop voltage during burn (see 18), and
C_{sawth} is an enhancement factor to account for sawtooth effects – although by default this factor is 1.

For a pulsed reactor the burn time is:

$$t_{burn} = \frac{\Phi_{burn}}{V_{burn}}$$

10. Radiation

In a reactor the power entering into the scrape-off layer must be kept to a minimum in order to protect the divertor. Introducing a large amount of impurity radiation is one way of achieving this goal. The model in PROCESS has recently been updated. The ratio of the density of each impurity to the electron density is assumed to be uniform throughout the plasma, and is set by the user. However, the user can optionally choose any one impurity fraction as an iteration variable to be adjusted by the code.

The radiation per unit volume is calculated using loss functions calculated by the code ADAS405 (25) – see Figure 7. The effective collisional–radiative coefficients which are required to establish the ionisation state and radiative losses of each ionic species, assuming equilibrium ionisation balance in optically thin plasma, were taken from the ADF11 derived data files (26). For H, He, Be, C, N, O, Ne and Si these use the generalized collisional-radiative approach (27). For Ni the data are based on (28), for Fe on (29), and for W see (30). The Ni and Fe rates have a density dependence imposed following the procedure in (31). The Kr and Xe data is from the ADAS baseline.

The resulting loss functions have a slow dependence on density, but are calculated at a fixed density (10^{19} electrons m^{-3}). This contrasts with strict coronal equilibrium, which is independent of density. In reality non-local effects due to density and temperature gradients will be significant, but these are not taken into account. The loss functions include both bremsstrahlung and line and recombination radiation, giving

$$P_i = n_i n_e L_Z(Z_i, T)$$

where P_i = radiation per unit volume (excluding synchrotron radiation),
$L_Z(Z_i, T)$ = loss function for ion species i at temperature T.
n_i = density of ion species i.

The radiation emission is integrated numerically over the plasma profile, using the temperature and density profiles. Only emission from within the separatrix is included, as PROCESS has no model for the scrape-off layer.

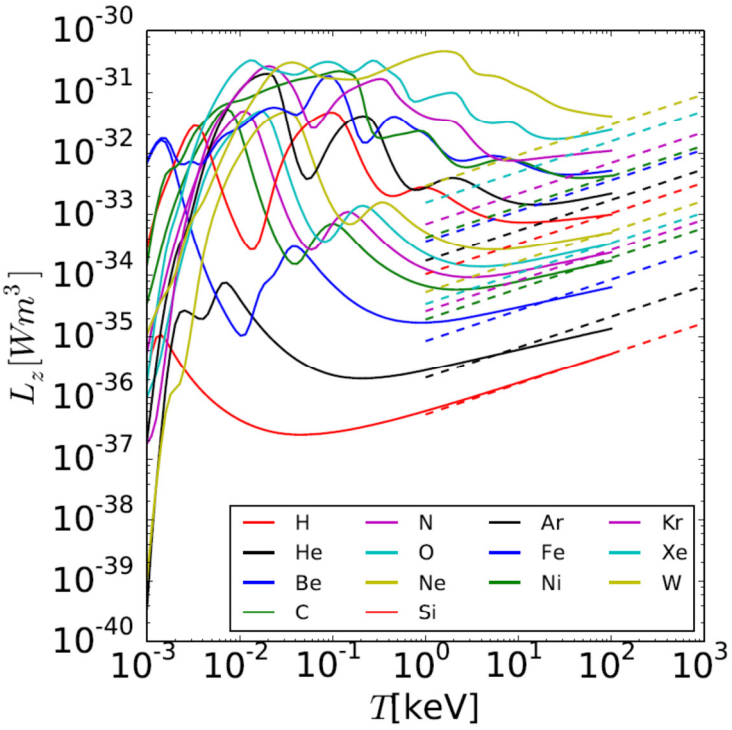

Figure 7. Radiation loss functions as a function of temperature, at 10^{19} electrons m^{-3}. The lowest line is H, with the other lines in the order listed. The dashed lines show the bremsstrahlung calculated using a separate method.

The plasma inside the separatrix is divided into the "core" and "edge", separated by a normalised minor radius set by the user. Radiation is calculated separately for core and edge, except for the synchrotron contribution, which is assumed to come from the core.

The calculation of synchrotron radiation is based on (32), which modifies the results of (33) taking reflections into account, and can conveniently be found in (4). This is currently based on a temperature profile different from the standard PROCESS options:

$$T_e(\rho) = (T_{0e} - T_{ea})\left(1 - \rho^{\beta_T}\right)^{\alpha_T} + T_{ea}$$

where α_T and β_T are peaking parameters for the electron temperature profile, T_{0e} is the central electron temperature and T_{ea} is the edge electron temperature. The edge electron temperature T_{ea} is fixed at 1 keV, and the peaking parameter for the electron temperature profile β_T is fixed as 2. (This makes the profile agree with the no-pedestal PROCESS profile, except for an overall shift equal to T_{ea}.) This is stated to be accurate (or at least a good fit to the detailed calculations) for:

$$10 < T_{e0} < 100 \text{ keV},\ 1 < \kappa < 2.5,$$
$$0 < \alpha_n < 2,\ 0 < \alpha_T < 8$$
$$1 < \beta_T < 8, \text{ and } 1.5 < 1/\varepsilon < 15.$$

The power loss from synchrotron radiation is strongly dependent on the reflectivity of the wall, which is poorly known and must be set by the user.

11. Fusion Power

The fusion reactions included are DT, DD (both branches), and D^3He. The volume-averaged thermal fusion power per unit volume from DT fusion is

$$P_{DT} = \langle \sigma v \rangle_{av} f_T f_D \langle n_f \rangle^2 E_t,$$

and similarly for the other reactions, taking account of the factor of ½ required for DD reactions.
where $\langle \sigma v \rangle_{av}$ = density-weighted mean DT fusion rate coefficient,

f_T = fraction of fuel ions that are tritium,
f_D = fraction of fuel ions that are deuterium,
f_{He3} = fraction of fuel ions that are ^{3}He,
E_t = energy released in D-T reaction,
$<n_f>$ = fuel ion density.

The mean fusion rate coefficient is calculated by integrating over the plasma profile. The result can be shown to be

$$\langle \sigma v \rangle_{av} = 2(1+\alpha_n)^2 \int_0^1 \rho(1-\rho^2)^{\alpha_n} \langle \sigma v \rangle(T)\, d\rho$$

where the fusion rate constants $<\sigma v>(T)$ is calculated at a temperature T given by

$$T = \langle T_i \rangle (1+\alpha_T)(1-\rho^2)^{\alpha_T}.$$

The rate constants are from the fitting of Bosch and Hale (34) (35), valid in the ion temperature range 0.2 – 100 keV. The total fusion power is divided into alpha and neutron power:

$$P_{owfmw} = (P_\alpha + P_{neut})V.$$

The alpha power derives from thermal fusion and beam-plasma fusion:

$$P_\alpha = P_\alpha(thermal) + \frac{P_{\alpha NB}}{V}$$

Even for the DEMO B model in section 26, which has 200 MW of injected deuterium atoms, beam-plasma fusion is only 2.5% of the total. The alpha power from beam-plasma fusion is

$$P_{\alpha NB} = f_{beamfus}(P_{\alpha DB} + P_{\alpha TB})$$

$f_{beamfus}$ = user-specified multiplier for beam-plasma fusion calculation,
$P_{\alpha DB}$ = alpha power from beam-plasma fusion due to deuterium beams,
$P_{\alpha TB}$ = alpha power from beam-plasma fusion due to tritium beams.

The cross-section for beam-background fusion cannot be derived from the fitting by Bosch and Hale, which does not cover the energy range required, so an alternative fit is used. The beam-plasma reaction rate coefficient is

$$\frac{\text{fusion rate}}{\text{background ion density} \times \text{beam ion density}} = \frac{3v_{crx}}{\ln\left(1+\left(\frac{v_{beam}}{v_{crx}}\right)^3\right)} \int_0^{\frac{E_{nbeam}}{v_{crx}}} \frac{u^3}{1+u^3} \sigma_{bmfus}(u)\, du$$

where E_{nbeam} = initial neutral beam energy, σ_{bmfus}= fusion cross-section. The variable of integration u is the ratio of beam ion velocity during slowing down to the critical velocity for electron/ion slowing down, v_{crx}. DD beam-plasma fusion is neglected.

12. Effective charge and impurities

Helium ash and other impurities will dilute the fuel. The density of fuel ions $\langle n_f \rangle$ follows from charge neutrality:

$$\langle n_f \rangle = \langle n_e \rangle - \langle n_{beam} \rangle - 2\langle n_{\alpha fast} \rangle - \langle n_e \rangle \sum_i f_i Z_i$$

where f_i is the number density of species i, as a fraction of the electron density, and Z_i is its atomic number,
$<n_{beam}>$ = hot beam ion density,
$<n_{\alpha fast}>$ = fast alpha density.
For this purpose all elements are assumed to be fully ionized. The effective charge, neglecting fast particles, can be shown to be:

$$Z_{eff} = \sum_i f_i Z_i^2$$

13. Plasma Current

The safety factor q_{95} required to prevent disruptive MHD instabilities (which is an input) dictates the plasma current I_p :

$$I_p = \frac{2\pi}{\mu_0} B_t \frac{a^2 f_q}{R q_{95}} .$$

The factor f_q makes allowance for toroidal effects and plasma shaping (elongation and triangularity). Several formulae for this factor are available, but the default is (19) (11),

$$f_q = \frac{1.17 - 0.65\varepsilon}{2(1-\varepsilon^2)^2}\left(1 + \kappa_{95}^2\left(1 + 2\delta_{95}^2 - 1.2\delta_{95}^3\right)\right).$$

14. Energy Confinement

14.1. Confinement scalings

Several empirical scaling relationships have been proposed for energy confinement, based on selected pulses from several different machines. We are faced with the task of extrapolating these to a reactor.

A reactor will require a large fraction of the alpha power from fusion to be radiated –preferably from the edge or the from the divertor region. Inevitably there will also be significant bremsstrahlung and synchrotron radiation from the core. This contrasts with the published scalings, which are derived from experiments with low radiation fraction. The effect of radiation on confinement is not well understood. It is likely that radiation from the outer part of the pedestal will not greatly affect the power conducted by ions and electrons from the core and the inner part of the pedestal. On the other hand, radiation from the central plasma and the inner part of the pedestal is almost certainly an additional loss mechanism to the conducted power. PROCESS allows for this by calculating energy loss from the confinement time, and then adding the radiation emitted within a user-defined radius referred to as the "core", as explained in section 10. The power lost by the plasma is therefore

$$P_{lost} = P_{scaling} + P_{core}$$

where the conducted loss from the confinement scaling is

$$P_{scaling} = \frac{W_{th}}{\tau_E}$$

W_{th} is the thermal energy of the plasma,
P_{core} is the radiation from the "core", and
τ_E is the energy confinement time derived from the scaling as below.

Differences may exist in the ways in which energy confinement time is defined and measured by different authors, but these are not significant compared to the uncertainty involved in extrapolation. The experimental scalings below are derived from the stored thermal energy only. Thus fast ion losses are taken as energy not deposited in the plasma, rather than as energy lost from the plasma, and PROCESS uses this same convention.

The radiation also has an influence on the right hand side of the confinement scaling equation, which includes the so-called "loss power" P_L, which we interpret as power transported out from the "core" by charged particles:

$$P_L = P_{inji} + P_{inje} + V\left(P_\alpha + P_{ohmpv} - P_{core}\right).$$

P_{ohmpv} = inductive heating power (called ohmic heating) per unit volume and the other symbols are in Table 2.

For high confinement mode operation (H-mode) with ELMs, the most commonly used scaling is based on IPB98(y,2) (36). The energy confinement time, averaged over the ELMs, is

$$\tau_E = H_{fact}\, 0.0562\,\mathrm{sec} \left(\frac{I_p}{MA}\right)^{0.93} \left(\frac{B_t}{T}\right)^{0.15} \left(\frac{\langle n_e\rangle_{la}}{10^{19} m^{-3}}\right)^{0.41} \left(\frac{P_L}{MW}\right)^{-0.69} \left(\frac{R}{m}\right)^{1.97} \kappa_a^{0.78} \epsilon^{0.58} A_{fuel}^{0.19}$$

where
H_{fact} = user-defined enhancement factor

κ_a = plasma elongation calculated as

$$\kappa_a = \frac{A_x}{\pi a^2}$$

A_x is the cross-sectional area inside the separatrix,

A_{fuel} = average mass of fuel portion of ions (amu),

Low confinement (L-mode) operation is sometimes considered for reactors as it has no ELMs. PROCESS offers several L-mode options, one of which is from Kaye *et al* (37):

$$\tau_E = H_{fact}\, 0.023\,\mathrm{sec} \left(\frac{I_p}{MA}\right)^{0.96} \left(\frac{B_t}{T}\right)^{0.03} \left(\frac{\langle n_e\rangle_{la}}{10^{19} m^{-3}}\right)^{0.40} \left(\frac{P_L}{MW}\right)^{-0.73} \left(\frac{R}{m}\right)^{1.83} \kappa_{95}^{0.64} \epsilon^{-0.06} A_{fuel}^{0.20}$$

14.2. L-H transition

H-mode can only be maintained if the "loss power" (the power transported by charged particles through the edge of the plasma) is sufficient to prevent reversion to L-mode. Several L-H threshold scalings for loss power are available – the default is from Martin *et al* (38), who used the international H-mode threshold power database. Martin's definition of loss power excludes the power loss by fast ions in unconfined orbits and charge-exchange processes.

$$P_{LH} = 0.0488 \left(\frac{\langle n_e\rangle_{la}}{10^{20} m^{-3}}\right)^{0.717} B_t^{0.803}\, S_{area}^{0.941}\, \frac{2}{A_{ion}}$$

(units MW, 10^{20} m^{-3}, T and m^2.) The symbols are:

S_{area} = plasma surface area (see 7),

A_{ion} = mean ion mass (amu), given by

$$A_{ion} = \frac{A_{fuel}\langle n_f\rangle + 4\langle n_\alpha\rangle + A_{beam}\langle n_{beam}\rangle + \langle n_e\rangle(12 f_C + 16 f_O + M_Z f_Z)}{\langle n_i\rangle}$$

A_{fuel} = average mass of fuel portion of ions (amu)

$\langle n_\alpha\rangle$ = thermal helium ion density

A_{beam} = beam ion mass (amu),

$\langle n_{beam}\rangle$ = hot beam ion density

$\langle n_i\rangle$ = total ion density

f_C , f_O , f_Z = impurity fractions (see 19),

M_Z = mass of high Z seeded impurity ion,

and other variables are in Table 3.

15. Definitions of β

The total plasma β is usually an iteration variable. Definitions of other forms of β are listed below, using the following quantities:

B_{tot} = total magnetic field (see below)

$\langle n_{it}\rangle$ = total ion density, including fuel and impurities

β_{fi} = fast alpha contribution to beta (section 17)

β_{NB} = fast beam ion contribution to beta (section 17)

P_{coef} = profile factor (see 4.1).

The poloidal magnetic field B_p averaged over the plasma perimeter is given by Ampère's law:

$$B_p = \frac{\mu_0 I_p}{L},$$

where L is the plasma perimeter, given in section 7. The total magnetic field B_{tot} is calculated as the vector sum of the toroidal field at the geometric axis and the poloidal field averaged over the perimeter,

$$B_{tot} \equiv \sqrt{B_t^2 + B_p^2}.$$

The poloidal β, based on the full plasma pressure including fast particles, is then scaled from the total β:

$$\beta_p = \beta \left(\frac{B_{tot}}{B_p}\right)^2.$$

Thermal β:

$$\beta_{th} = 2\mu_0 \mathrm{e}\ P_{coef} \frac{\langle n_e \rangle \langle T_e \rangle + \langle n_{it} \rangle \langle T_i \rangle}{B_{tot}^2}$$

Toroidal β:

$$\beta_t = \beta \left(\frac{B_{tot}}{B_t}\right)^2$$

Thermal poloidal β:

$$\beta_{p,thermal} = (\beta - \beta_{ft} - \beta_{NB}) \left(\frac{B_{tot}}{B_p}\right)^2$$

The relationship between the different contributions to beta must be applied as a constraint:

$$\beta = \beta_{ft} + \beta_{NB} + \frac{2\mu_0 e}{B_{tot}^2} (\langle n_e \rangle \langle T_e \rangle_n + \langle n_{it} \rangle \langle T_i \rangle_n)$$

Two alternative values of "normalised beta" are calculated, irrespective of the beta limit option chosen:

$$\beta_N(\%) = \frac{\beta}{0.01 \frac{I_p}{aB_t}}$$

and

$$\beta_{thermalN}(\%) = \frac{\beta - \beta_{ft} - \beta_{NB}}{0.01 \frac{I_p}{aB_t}}.$$

16. β and density limits

Three options are available for implementing the beta limit (all using MA, m, Tesla).

Option 1 (the default): Includes all beta components:

$$\beta \leq 0.01\, g \frac{I_p}{aB_t}.$$

Option 2: Here, the beta limit applies only to the thermal component of beta, not the fast alpha or neutral beam parts:

$$\beta - \beta_{ft} - \beta_{NB} \leq 0.01\ g \frac{I_p}{aB_t}.$$

For this option a user-defined limit can also be applied to $\varepsilon\beta_p$.

Option 3: Here the beta limit applies to combined thermal and neutral beam components of the total beta, but excludes the contribution due to the fast alphas:

$$\beta - \beta_{ft} \leq 0.01\ g \frac{I_p}{aB_t}.$$

By default the value of g is set by the user. Alternatively it can be calculated from the aspect ratio using

$$g = 2.7(1 + 5\epsilon^{3.5})$$

(which gives g = 3.0 for aspect ratio = 3), or using

$$g = 4l_i\,.$$

Several different plasma density limits are available (20). The simplest is the Greenwald limit, given by

$$n_G = 10^{14} \left(\frac{m^{-3}m^2}{Amp}\right) \quad \frac{I_p}{\pi a^2}$$

In this case the limit applies to the line-averaged electron density, not the volume-averaged density.

Both the density limit and the beta limit are available as constraints. As always, all the constraints specified by the user are imposed simultaneously.

17. Fast ions

The fast alpha particles and beam ions will make a substantial contribution to the total plasma pressure. The fast alpha contribution to beta, β_{ft}, is given (by default) by a fit based on (39), but taking into account the deviation of the fusion cross-section from T^2 dependence at high temperatures.

$$\beta_{ft} = \beta_{th}\left(\frac{P_\alpha}{P_\alpha - \frac{P_{\alpha NB}}{V}}\right) \times the\ smaller\ of \left\{ 0.3 \atop 0.26\left(\frac{\langle n_i\rangle}{\langle n_e\rangle}\right)^2\left(P_{coef}\frac{\langle T_i\rangle + \langle T_e\rangle}{20\ keV} - 0.65\right)^{0.5}\right\}$$

where
β_{th} = thermal beta (see 15)
P_α is the fusion alpha power per volume,
$P_{\alpha NB}$ is the α power from fusion due to fast beam ions, and
P_{coef} is the profile factor (see 3 above).

The contribution to β by fast beam ions is:

$$\beta_{NB} = \frac{2}{3}4.03\times10^{-22}\frac{\beta_{bm0}\langle n_{beam}\rangle E_{hotNB}}{B_{tot}^2}$$

where β_{bm0} =1.5 by default, and $<n_{beam}>$ and E_{hotNB} are the average density and energy of the fast beam ions. The average fast ion energy is derived based on (40). The fast beam ion density is the sum of the deuterium and tritium components:

$$\langle n_{beam}\rangle_D = (1 - f_{tritbm})I_{beam}\frac{\frac{\tau_{sbme}}{3}\ln\left(1 + \left(\frac{E_{nbeam}}{E_{critD}}\right)^{1.5}\right)}{V}$$

$$\langle n_{beam}\rangle_T = f_{tritbm}I_{beam}\frac{\frac{\tau_{sbme}}{3}\ln\left(1 + \left(\frac{E_{nbeam}}{E_{critT}}\right)^{1.5}\right)}{V}$$

where f_{tritbm} = fraction of beam that is tritium,
I_{beam} = rate at which neutral beam atoms enter the plasma,
E_{nbeam} = neutral beam energy,
τ_{sbme} = beam ion slowing down time, given in this module by

$$\tau_{sbme} = 1.99\times10^{19}\,(2(1 - f_{tritbm}) + 3f_{tritbm})\frac{\langle T_e\rangle_n^{1.5}}{\langle n_e\rangle\Lambda_{ie}}$$

E_{critD} and E_{critT} are the critical energies (at which the ions and the electrons are heated equally by the beam ion) for D and T respectively, given by

$$E_{critD} = 14.8\langle T_e\rangle_n\,2\langle Z_{eff}\rangle_n^{2/3}\frac{(\Lambda_{ie} + 4)}{\Lambda_{ie}}$$

$$E_{critT} = \frac{3}{2}E_{critD}$$

The density of fast beam ions (relative to the electron density) is always an iteration variable, and the following consistency equation must be applied:

$$\langle n_{beam}\rangle = \langle n_{beam}\rangle_D + \langle n_{beam}\rangle_T$$

(Units in this section are s, keV,Tesla, m^{-3}. $<Z_{eff}>_n$ and the Coulomb logarithm Λ_{ie} are given above.)

18. Plasma loop resistance and ohmic heating

The plasma loop resistance is:

$$\rho_{plas} = 2.15 \times 10^{-9} ohm \cdot m \quad \frac{Z_{eff} R}{\kappa a^2 \left(\frac{\langle T_e \rangle}{10\ keV}\right)^{3/2}} \left(4.3 - 0.6\frac{R}{a}\right)$$

The expression is suitable for $\alpha_n = 0.5$, $\alpha_T = 1.0$, $\alpha_J = 1.5$. The second factor is the so-called neo-classical resistivity enhancement caused by particle trapping (11), valid for aspect ratios in the range 2.5–4. An additional enhancement due to sawtooth effects can be added later.

Loop voltage during burn is

$$V_{burn} = I_p \rho_{plas} f_{acoh},$$

where f_{acoh} = the fraction of plasma current produced inductively. The resistive (ohmic) heating power per unit volume is therefore

$$P_{ohmpv} = \frac{f_{acoh} I_p^2 \rho_{plas}}{V}.$$

19. Energy gain and power balance

The fusion energy gain Q is defined as

$$Q = \frac{P_{owfmw}}{P_{inje} + P_{inji} + P_{ohmpv}},$$

Power to the divertor will depend on the power transported through the separatrix by charged particles,

$$P_{sep} = P_\alpha V + P_{inji} + P_{inje} + P_{ohmpv} V - P_{rad}$$

No detailed divertor model is in use at present. Instead a simple constraint can be applied to the ratio P_{sep}/R.

The following constraints can be imposed.

Ion power balance:

$$P_{tri} + P_{ie} = F_\alpha P_{\alpha i} + \frac{P_{inji}}{V},$$

electron power balance:

$$P_{tre} + P_{rad} = F_\alpha P_{\alpha e} + P_{ie} + \frac{P_{inje}}{V},$$

and total power balance:

$$P_{lost} = F_\alpha P_\alpha V + P_{ohmpv} V + P_{inji} + P_{inje}\ .$$

In this section,

P_{owfmw} = total fusion power

P_{sep} = power transported through the separatrix by charged particles

and the remaining quantities are all volume-averages, per unit volume of plasma:

P_{ohmpv} = Inductive heating power (called ohmic heating)

P_{tre} = electron transport power through separatrix

P_{tri} = ion transport power through separatrix

P_{ie} = power from ions to electrons,

$P_{\alpha e}$ = alpha power to electrons

$P_{\alpha i}$ = alpha power to ions

P_{rad} = total radiation power from the confined plasma

F_α = fraction of alpha power deposited in the plasma

P_{lost} = power lost by the plasma (section 14.1)

20. Optimisation

In optimisation mode PROCESS uses the routine VMCON, based on a variable metric method by Powell (41) (42), which finds a stationary point of a function (the figure of merit), consistent with a general set of equality and inequality constraints. The derivative of the function must be available, and is calculated using finite differences. The second derivative does not need to be provided, but a matrix related to it is estimated by the algorithm. A Lagrange function is created using Lagrange multipliers. The stationary point of the Lagrange function is found by a variant of the BFGS method (43). At each stage in the iteration this function is modelled as a quadratic in the vicinity of an initial trial point in parameter space. A line search algorithm then seeks an approximate minimum of the Lagrange function along the vector joining the trial point with the minimum of the quadratic. A recent addition to PROCESS enables the optimisation procedure to continue even if the line search fails. No attempt is made to ensure that a global minimum is found.

21. Application to ITER and DEMO

21.1. Comparison with detailed ITER calculations

The predictive capabilities of PROCESS in plasma physics are, unsurprisingly, limited. It must be remembered that the main aim of a systems code is to combine engineering, physics and economics. Table 5 gives the parameters of a model which shows the main plasma features of an inductive ITER scenario (44). The density and temperature profile exponents with no pedestal (see 4) were adjusted manually to achieve the same fusion power (400 MW) and effective charge (1.66), resuting in $\alpha_n = 0.45$, $\alpha_T = 0.25$.

Table 5. (A) Input parameters in process set equal to ITER scenario (44).

Parameter	Value
R (m)	6.2
a (m)	2.0
B_T (T)	5.3
q_{95}	3.0
κ_{95}	1.70
δ_{95}	0.33
$<n_e>$ $10^{19}m^{-3}$	10.1
$<T_i>$	8.0
P_{NB} (MW)	33
P_{RF} (MW)[a]	7
f_{He} = He density / ion density (average) (%)	3.2
f_{Be}	2.0
f_{Ar} (%)	0.12
Beam tangency radius (m)	5.31

[a] In PROCESS simultaneous RF and NB heating are not allowed. The RF heating was assumed to be additional unspecified heating with no current drive.

(B) Results. Those differing by more than 20% are shown in *italics*. The complete output file is available in Supplementary Information.

Parameter	ITER	PROCESS
Volume (m^3)	831	845
Surface area (m^2)	683	697
Poloidal perimeter (m)	18.2	18.4
Poloidal cross-section (m^2)	21.9	22.2
I_p	15.0	15.06
l_i	0.84	*0.65* [a]
V_{loop} loop voltage (mV)	75	*98.5*
β_N Normalised beta	1.8	1.76
β_T Toroidal beta (%)	2.5	2.60
β_p Poloidal beta	0.65	0.69
$<T_e>$ (keV)	8.8	8.0 [b]
P_{OH} Inductive heating (MW)	1	*1.48*
P_{SYN} Net synchrotron loss (MW)	8	*2.8*
P_{RAD} Total radiation (MW)	47	37.8
τ_E Energy confinement time (s)	3.7	4.22
W_{th} plasma thermal energy (MJ)	320	330
W_{fast} fast particle energy energy (MJ)	32	37
τ_{He} / τ_E	5	4.58 [c]
Beam-driven current (MA)	1	0.888
Bootstrap current (MA)	2.2	*4.44*

[a] default value

[b] PROCESS is normally used with equal electron and ion temperatures.

[c] PROCESS has only a single particle confinement time.

The biggest fractional discrepancy is a factor of three in the net synchrotron loss power, but the reason for this is not understood at present. The bootstrap current model, which disagrees by a factor of two, is being replaced (section **Error! Reference source not found.**). There is a 48% discrepancy in the inductive heating power (known as ohmic heating), but the absolute value of this power is very low. Note that the results are far from unique – the same specified conditions could be achieved using other combinations of inputs, some of which might lead to closer agreement with the results of detailed calculations. PROCESS is not a plasma scenario code.

21.2. Latest DEMO models

The high-level objectives proposed for a fusion power plant "DEMO" are to produce significant electrical power for a significant length of time, to demonstrate tritium self-sufficiency, and to provide proof-of-principle for all technologies required for a commercial fusion power plant. Two new models for DEMO have been obtained using PROCESS (45). The first, DEMO A, is intended to be "conservative" in that it might be possible to build it using the technology of the near future. For example, the line-averaged electron density is 20% higher than the Greenwald limit, because this limit is thought to be based on the density near the edge, while the line-averaged density will be enhanced by the peaking of the profile expected at the low collisionality due to the high temperature. The energy confinement time is 10% higher than the IPB98(y,2) scaling law, approximately compensating for the radiation correction described in section 14. Since current drive technologies are not yet mature, only 12% of the current is assumed to be due to current drive. Consequently it is a pulsed machine, able to burn for only 1.65 hours at a time.

Despite the comparatively large size (major radius is 9 m), the fusion power is only 1.95 GW. The assumed gross thermal efficiency is 33%, giving just 465 MW net electric power. (A modest extrapolation of DEMO A is possible, with the same geometric features, extending the pulse operation length with some current-drive. Since a pulsed DEMO would in any event require about 100 MW additional heating to achieve H-mode, and would have the systems available, it seems reasonable to explore the performance of such a device.)

The second, DEMO B is intended to be "advanced" in that more optimistic assumptions are made. Figure 8 and Table 6 compare DEMO A and B with a reference ITER scenario, showing that current drive and bootstrap fraction need the most extrapolation. The high energy confinement H factor used for DEMO B is motivated by data suggesting that the standard scaling is unduly pessimistic at high β_N (46). The DEMO models in this section and the next were created using an older version of PROCESS (version 246).

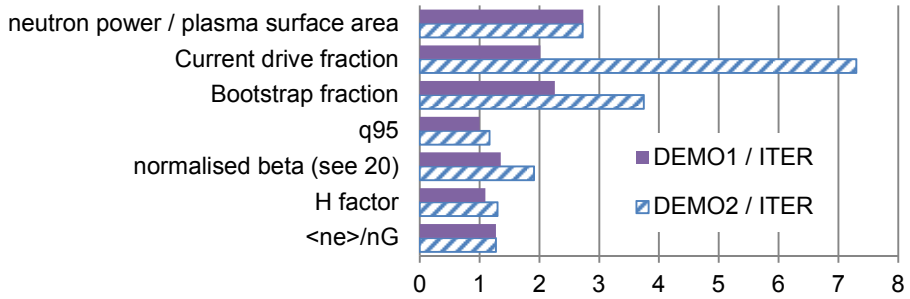

Figure 8. Comparison of DEMO A and B, both normalised to the 400 MW fusion power inductive ITER scenario. nG = Greenwald density (section 16)

Table 6 Comparison of DEMO A and DEMO B with the 400 MW fusion power inductive ITER scenario **(44)**

	ITER	DEMO A	DEMO B
$<n_e>/n_G$	0.85	1.081	1.08
H(IPB98(y,2)) H_{fact}	1.0	1.1	1.3
β_N (see 15)	1.8	2.44	3.44
q_{95}	3.0	3.0	3.5
Bootstrap fraction	15%	33.9%	56.2%
Current drive fraction	6.0%	12.1%	43.8%

21.3. Aspect ratio and burn time

In a self-consistent model the effect of varying the aspect ratio depends on a number of physics and engineering relationships (47). Figure 9 shows that for DEMO 1 as the aspect ratio is increased at constant pulse length the plasma volume initially decreases, so to maintain a constant fusion power the plasma density and the toroidal field increase, causing the TF coil to become much thicker. Up to an aspect ratio of about 3.5, the extra space available on the inboard side allows the major radius to remain constant, but beyond this point it must increase.

Figure 10 shows that as the required burn time increases the major radius increases (because of the space required for the central solenoid). Figure 11 shows the effect of allowing the aspect ratio to vary in order to minimise the major radius, but the optimum aspect ratio is somewhat erratic – probably because the minimum (shown in Figure 9) is so flat.

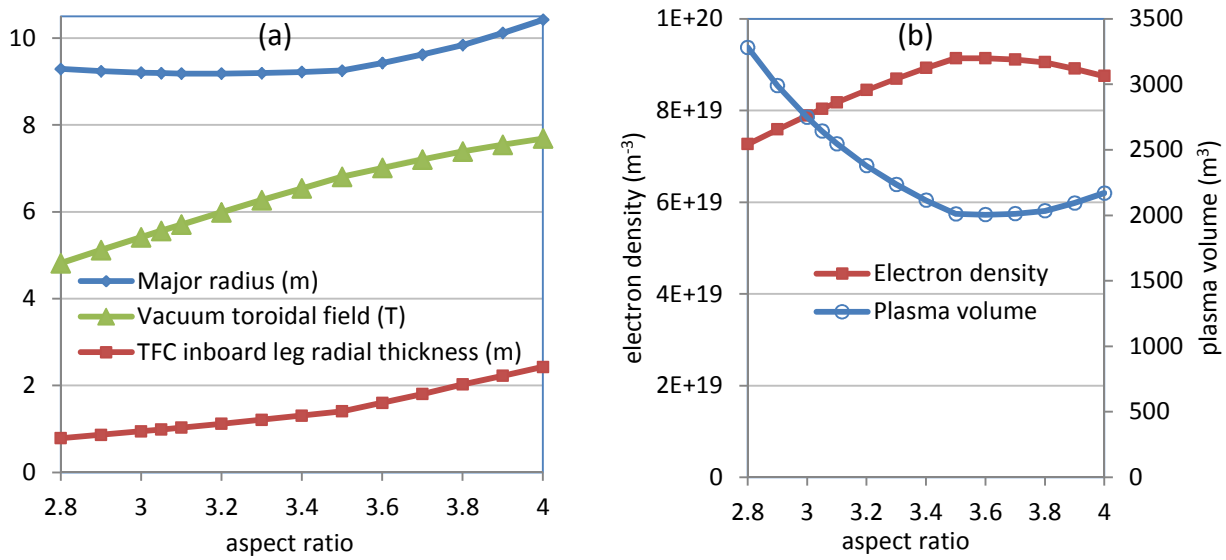

Figure 9. Parameters as a function of aspect ratio for DEMO 1, using PROCESS. The major radius was minimised. Net electric power = 500 MW, burn time = 2 hours.

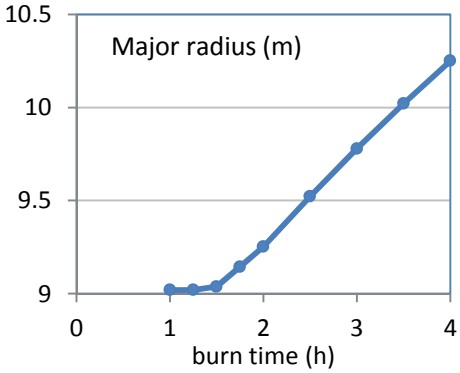

Figure 10. Major radius as a function of burn time for DEMO 1, using PROCESS, with fixed aspect ratio = 3.5. The major radius was minimised. Net electric power = 500 MW.

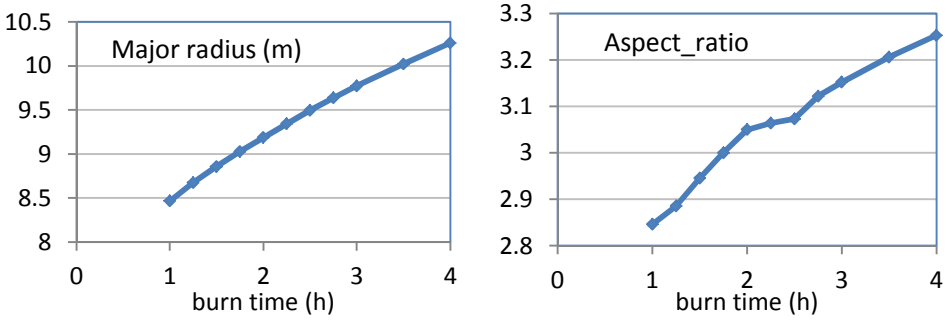

Figure 11. Parameters as a function of burn time for DEMO 1, using PROCESS. The aspect ratio and other variables were varied to minimise the major radius. Net electric power = 500 MW.

22. Discussion and Future work

Nakamura *et al* have compared the results from an earlier version of PROCESS and the Japanese code TPC, concentrating on the plasma physics (48). They found that once the plasma geometry, temperature, profile indices, and impurity fractions are defined, and a suitable figure of merit and constraint set are chosen for PROCESS, the other key plasma parameters derived by the two codes are in very good agreement – within about 5%, and usually much better. The exception is the radiation, which is very sensitive to the assumptions made concerning the pedestal and scrape-off layer. Kemp *et al* (49) discuss the discrepancies between the two sets of results, including the fast particle contribution to the plasma pressure, and the significant effect that different radiation models have on the confinement time.

In our view a systems code should do all the following things:

- Estimate cost of electricity
- Estimate safety parameters such as tritium inventory and tritium releases
- Optimise the design
- Include all known quantifiable constraints
- Make it possible for users to assess the scenario against constraints that are not yet quantified
- Show the assumptions
- Show dependence of results on assumptions
- Be up-to-date
- Be able to be compared with other systems codes
- Give scenarios that can be studied with detailed models.

It is desirable that it should

- Allow the source code to be read and checked.
- Allow the input and output files to be shared by other codes.
- Be rigorously tested
- Find the globally optimum design.

No systems code meets all these requirements yet. PROCESS is under active development –the pedestal, new radiation model and improved treatment of TF coil ripple were introduced recently, and new engineering and cost models are also being introduced. Work has begun on ensuring that results represent a global rather than just a local optimum, and on a user interface. The PROCESS homepage is www.ccfe.ac.uk/powerplants.aspx, and this includes a complete list of input parameters and their default values. A paper on the engineering and economic modules is in preparation. New algorithms can easily be incorporated, and we invite collaboration.

23. Acknowledgments

We would like to thank J. D. Galambos, P. C. Shipe, Y-K. M. Peng, R. Hancox, N. Taylor, R. Forrest, I. Cook, J. Hicks, C. Gardner, T. Hender, T. Todd, J. C. Rivas, F. Warmer, F. Franza, T. Hartmann, M. Nakamura, T. Goto, T. Miller, and all those who contributed to the TETRA code (2). Martin O'Mullane generated the radiation loss functions. This project has received funding from the European Union's Horizon 2020 research and innovation programme under grant agreement number 210130335, and from the RCUK Energy Programme [grant number EP/I501045]. The views and opinions expressed herein do not necessarily reflect those of the European Commission. To obtain further information on the models underlying this paper please contact the authors, or PublicationsManager@ccfe.ac.uk.

24. References

1. D. Maisonnier et al, Power plant conceptual studies in Europe, Nucl. Fusion 47 (2007) 1524–1532.
2. R.L. Reid et al, ETR/ITER Systems Code, ORNL/FEDC-87/7 (1988), https://engineering.purdue.edu/CMUXE/Publications/AHR/R88ORNL-FEDC-87-7.pdf.

3. P. J. Knight, A User's Guide to the PROCESS Systems Code, http://www.ccfe.ac.uk/assets/Documents/Other/PROCESS User Guide.pdf.
4. J. Johner, Helios: a zero-dimensional tool for next step and reactor studies, Fusion Science and Technology 59 (2011) 308.
5. T. Hartmann, Development of a systems code to assess implications of physics assumptions on the design of a demonstration fusion power plant (DEMO), dissertation at the Technische Universität München (2013).
6. Jaboulay, J-C., A. Li Puma, and J. Martínez Arroyo. Neutronic predesign tool for fusion power reactors system assessment. Fusion Engineering and Design (2013), http://dx.doi.org/10.1016/j.fusengdes.2013.05.082.
7. J. Wesson, Tokamaks, 3rd ed., Clarendon Press, Oxford (2004).
8. N.A. Uckan, Relative merits of size, field and current on ignited tokamak performance, Fusion technol., 14, p. 299 (1988).
9. http://www.netdenizen.com/emagnettest/offaxis/?offaxisloop.
10. M. Wilson, Superconducting Magnets, Clarendon Press, Oxford, N.Y., 1983, eq. 3.2 and fits to graph 3.3.
11. ITER Physics Design Guidelines: 1989, N.A. Uckan and the ITER Physics Group, ITER Documentation Series No. 10, IAEA, Vienna 1990, IAEA/ITER/DS/10.
12. *Neoclassical conductivity and bootstrap current formulas for general axisymmetric equilibria and arbitrary collisionality regime, Phys. Plasmas 6, 2834 (1999); doi: 10.1063/1.873240.* O. Sauter, C. Angioni, and Y. R. Lin-Liu.
13. T. Oikawa et al, Benchmarking of Neutral Beam Current Drive Codes as a Basis for the Integrated Modeling for ITER,IT/P6-5, http://www-naweb.iaea.org/napc/physics/FEC/FEC2008/papers/it_p6-5.pdf. Note that the model used appears to be ITER scenario 1, not 4 as stated : s.n.
14. A.R. Polevoi, S.Yu. Medvedev, V.D. Pustovitov, V.S. Mukhovatov, M. Shimada, Possibility of Q > 5 Stable, Steady-State Operation in ITER with Moderate beta-N and H-factor, Proc. 19th IAEA Fusion Energy Conf. (2002) IAEA-CN-94/CT/P-08. [Online] http://www-pub.iaea.org/MTCD/Publications/PDF/csp_019c/pdf/ctp_08.pdf.
15. D.R. Mikkelsen and C.E. Singer. Optimization of steady-state beam-driven tokamak reactors, Nucl. Technol./Fusion, 4, 237 (1983).
16. R.K. Janev, C.D. Boley, D.E. Post, Penetration of energetic neutral beams into fusion plasmas, 1989 Nucl. Fusion 29, 2125. equations 24, 25 and 26.
17. N. A. Uckan et al, Influence of fast alpha diffusion and thermal alpha buildup on tokamak reactor performance, Fusion Technology 13 (1988) p.411, cited by [13].
18. W. M. Nevins et al, Summary Report: ITER Specialists' Meeting on Heating and Current Drive, ITER-TN-PH-8-4, June 1988, Garching, FRG (This reference is included for historical completeness but no copy is known to exist.).
19. The physics of magnetic fusion reactors, J. Sheffield, Rev. Mod. Phys. , Yol. 66, No. 3, July 1994.
20. T. C. Hender, M. K. Bevir, M. Cox, R. J. Hastie, P. J. Knight, C. N. Lashmore-Davies, B. Lloyd, G. P. Maddison, A. W. Morris, M. R. O'Brien, M. F. Turner and H. R. Wilson, "Physics Assessment for the European Reactor Study", AEA Fusion Report AEA FUS 172.
21. Karney and Fisch, Efficiency of current drive by fast waves, Physics of Fluids (1958-1988) 28, 116 (1985) and 10.1063/1.865191, doi:.
22. ITER poloidal field system, IAEA Vienna (1990) pp. 203-30, 56-60.
23. Formulas and tables for the calculation of mutual and self-inductance [Revised], Rosa and Grover, Scientific papers of the Bureau of Standards, third ed., 1916.
24. S. P. Hirshman and G. H. Neilson, External inductance of an axisymmetric plasma, Phys. Fluids 29, 790 (1986) and doi:10.1063/1.865934, eq 14a, 15a and 15b.
25. www.adas.ac.uk.
26. http://open.adas.ac.uk/.
27. *Ionization state, excited populations and emission of impurities in dynamic finite density plasmas: I. The generalized collisional–radiative model for light elements.* Summers, H. P., Dickson, W. J., O'Mullane, M. G., Badnell, N. R., Whiteford, A. D., Brooks, D. H., … Griffin, D. C. Vols. Plasma Physics and Controlled Fusion, 48(2), 263–293. doi:10.1088/0741-3335/48/2/007.
28. Arnaud, M., and R. Rothenflug. "An updated evaluation of recombination and ionization rates." Astronomy and Astrophysics Supplement Series 60 (1985): 425-457.
29. Arnaud, M., and J. Raymond. "Iron ionization and recombination rates and ionization equilibrium." The Astrophysical Journal 398 (1992): 394-406.
30. Pütterich, T., et al. "Modelling of measured tungsten spectra from ASDEX Upgrade and predictions for ITER." Plasma Physics and Controlled Fusion 50.8 (2008): 085016.

31. H. P. Summers. Tables and graphs of collisional dielectronic recombination and ionisation equilibria of H-like to A-like ions of elements. IM-367, Appleton Laboratory, 1974.
32. Fidone, Giruzzi, Granata, Synchrotron radiation loss in tokamaks of arbitrary geometry, Nucl. Fusion 41 no. 12 (2001), p. 1755.
33. Albajar, Johner, Granata, Improved calculation of synchrotron radiation losses in realistic tokamak plasmas, Nucl. Fusion 41 no. 6 (2001), p 665. Equations 13, 15 and the two on page 674.
34. Bosch and Hale, Improved formulas for fusion cross-sections and thermal reactivities, (1992) Nucl. Fusion 32, 611, and erratum (1993) Nucl. Fusion 33, 1919.
35. Hartwig, Z. S. and Podpaly, Y.A., The Magnetic Fusion Energy Formulary, PSFC/RR-11-13 (2012).
36. Chapter 2: Plasma confinement and transport, ITER Physics Expert Groups on Confinement and Transport and Confinement Modelling and Database, and ITER Physics Basis Editors, 1999 Nucl. Fusion 39 2175.
37. Kaye and the ITER confinement database working group, ITER L mode confinement database, 1997 Nucl. Fusion 37 1303.
38. Martin et al, Power requirement for accessing the H-mode in ITER , equation 2, 11th IAEA Tech. Meeting on H-mode Physics and Transport Barriers, Journal of Physics: Conference Series 123 (2008) 012033.
39. N.A. Uckan, J.S. Tolliver, W.A. Houlberg and S.E. Attenberger, Influence of fast alpha diffusion and buildup on tokamak reactor performance, Fusion technology 13 411 (1988).
40. Deng, B. Q. and G. A. Emmert. Fast ion pressure in fusion plasmas. University of Wisconsin Fusion Technology Institute Report, UWFDM-718 (1987).
41. MJD Powell, A fast algorithm for nonlinearly constrained optimization calculations, Lecture notes in mathematics, p.144, Springer (Berlin) 1978.
42. Nuclear Energy Agency, NESC0922 VMCON.http://www.oecd-nea.org/tools/abstract/detail/nesc0922/.
43. [Online]
http://en.wikipedia.org/wiki/Broyden%E2%80%93Fletcher%E2%80%93Goldfarb%E2%80%93Shanno_algorithm.
44. Plasma Performance Assessment, ITER_D_22HGQ7 (2009), Table 3.1-1.
45. www.ccfe.ac.uk/powerplants.aspx.
46. D.J. Ward, The physics of DEMO, Plasma Phys. Control. Fusion 52 (2010) 124033.
47. J.-L. Duchateau∗, P. Hertout, B. Saoutic, P. Magaud, J.-F. Artaud, G. Giruzzi, J. Bucalossi, J. Johner,P. Sardain, Conceptual design for the superconducting magnet system of a pulsed DEMO reactor,Fusion Engineering and Design 88 (2013) 1609– 1612.
48. Nakamura, Makoto, Richard Kemp, Hiroyasu Utoh, David J. Ward, Kenji Tobita, Ryoji Hiwatari, and Gianfranco Federici. "Efforts towards improvement of systems codes for the Broader Approach DEMO design." Fusion Eng. and Design 87, no. 5 (2012): 864.
49. Kemp, R., Nakamura, M., Ward, D. J., Tobita, K., & Federici, G. Benchmarking reactor systems studies by comparison of EU and Japanese system code results for different DEMO concepts. In 24th IAEA Fusion Energy Conference (IAEA FEC 2012).
50. H. Zohm et al, On the Physics Guidelines for a Tokamak DEMO, FTP/3-3, Proc. IAEA Fusion Energy Conference 2012, October, San Diego.
51. J. Johner, R. Kemp, T. Hartmann, and D. Ward, HELIOS / PROCESS / IPP Benchmarks: Draft-Version of 15/11/11. Private Communication.
52. R.H. Cohen, Effect of trapped electrons on current drive, Phys. Fluids, 30, 2442 (1987) and erratum Phys. Fluids, 31, 421 (1983).
53. H.R. Wilson, Bootstrap current scaling in tokamaks, 1992 Nucl. Fusion 32 257,.
54. S. P. Hirshman, Finite-aspect-ratio effects on the bootstrap current in tokamaks, Phys. Fluids 31 (10) (1988), p. 3150.
55. HSL Archive, Science and Technology Facilities Council, http://www.hsl.rl.ac.uk/archive/.